 CMES, vol.6, no.4, pp.333-347, 2004

Analysis of Particulate Composite Materials Using an Element Overlay Technique

H. Okada[1], C. T. Liu[2], T. Ninomiya[1], Y. Fukui[1] and N. Kumazawa[1]

Abstract: Formulations and applications of an element overlay technique for the mesoscopic analyses of composite structures are presented in this paper. As a zooming technique, the element overlay technique has been applied to various engineering problems. A finite element mesh having finer mesh discretization is superposed at the region to zoom the spatial resolution of analysis. Such a numerical technique is known as the s-version FEM (S-FEM). This paper aims at developing an S-FEM technique that is suited for the mesoscopic analysis of particulate composite materials. Local finite element models that contain the second phase material and its immediate vicinity are superposed on global finite element model. Each local finite element model contains only one particle and is relative to simple to build. The global finite element model does not model particles at all. To distribute a number of particles in the analysis region, we place the local finite element model at the location of particles, just by specifying their locations. The local and global finite element models are built independently. Building and modifying an analysis model is much simpler than the case of an ordinary finite element method. Mathematical formulations, computational strategies and some numerical examples are presented for the problems of distributed holes/voids and particles. The same analysis technique can be applied to other types of composite structures.

keyword: Particulate composite material, s-version FEM (S-FEM), Finite Element Method (FEM).

1 Introduction

In this paper, an element overlay technique is applied to the analyses of particulate composite materials. For the analyses of heterogeneous solid, such as particulate composite materials, unit cell analyses have typically been performed with assuming a very small number of reinforcing particles in the analysis region [see, for example, a review paper of computational micromechancis by Needleman (1989)]. Such analyses inherently assume that the particles are placed in a periodic manner. It was concluded in Matsuda, Ohno, Tanaka and Shimizu (2003) that the macroscopic behavior of the composite is not influenced by the randomness but the microscopic stress distribution largely depend on the arrangement of particles. According to literature [Lee, Moorthy and Ghosh (1999), Zhong and Knauss (2000)], for the analyses of progressive material damage, it is very important to account for the randomness in particle distribution. In order to model the randomness explicitly, it is obvious that many particles need to be included in the material model. When a large number of particles are assumed, the analysis models would become very large and complex, especially in three-dimensional cases. Though excellent numerical techniques based on the finite element method such as Voronoi cell FEM [Lee, Moorthy and Ghosh (1999), Raghavan and Ghosh (2004)] have been proposed by researchers, but most of applications are confined in two-dimensional ones. Recently, finite element analyses that explicitly model distributed particles in a three-dimensional unit cell were presented by Böhm, Eckschlager and Han (2002) and Böhm, Han and Eckschlager (2004). They included about 15 particles in the unit cell. It is however seem to be very troublesome to build such models.

In order to carry out three-dimensional analysis for the problems of particulate composite materials with a large number of randomly distributed particles, present authors have sought some alternating computational methods other than the conventional finite element method. Okada, Fukui and Kumazawa (2004) presented a boundary element based computational method, in which the distributed particles were modeled by using the analytical solutions for ellipsoidal particles [see Mura (1982) for the analytical solutions]. The modeling strategy was in success as long as matrix material is elastic. The authors extended the method to model the material nonlinear be-

[1] Kagoshima University, Kagoshima, Japan
[2] AFRL/PRSB, Edwards AFB, USA

havior due to particle damages [see, Okada, Fukui and Kumazawa (2003a) for particle fracture and the phase transformation of the particles and Okada, Fukui and Kumazawa (2003b) for the cavitation of rubber particles in modified epoxy-resin].

However, when matrix material undergoes any nonlinear deformation, the efficiency of the BEM approach diminishes. Thus, present authors sought a methodology that allows an analyst to build analysis model as quickly as the boundary element approach of Okada, Fukui and Kumazawa (2004) and S-version finite element method (S-FEM; an element overlay technique) was found to have very attractive features. In S-FEM analyses, a finite element model is superposed on another finite element model and they are generated independently. Therefore, it is very tractable to build an analysis model. The S-FEM was first presented by Fish (1992) and was applied to various problems [Fish, Markolefas, Guttal and Nayak (1994)] as a zooming technique that enhances the spatial resolution of discretization locally. Then the method was applied to the problems of composite plate in Fish and Guttal (1996). Takano, Zako and Ishizono (2000) applied the S-FEM technique to compute the stress distributions of heterogeneous material by enhancing the spatial resolution locally using an overlaid finite element model. Nakasumi, Suzuki, Fujii and Ohtsubo (2003) solved the problems of shell and plate structure by superposing solid elements on shell/plate elements. Lee, Song, Yoon, Zi and Belytschko (2004) combined the S-FEM approach with extended finite element method [X-FEM, Moës, Dolbow and Belytschko (1999)]. Okada, Endoh and Kikuchi (2004) solved linear fracture mechanics problems and a simple criterion to guarantee the accuracy of evaluated crack tip parameters. It should be noted that other attractive ways to attack the problems of particulate composite materials would be in the adaptive mesh-refinement in finite element analysis [Chung, Choi and Kim (2003)] and in the adaptive node-refinement in meshless local Petrov-Galarkin (MLPG) method [see Atluri and Shen (2002) and Atluri (2004) for the comprehensive descriptions of MLPG]. MLPG with an adaptive node-refinement was presented by Kim and Atluri (2000).

So far, the element overlay technique had mainly been used as a method to locally enhance the spatial resolution of discretization. In present investigation, the element overlay technique is applied to the problems of particulate composite materials. Analysis model has a number of particles as shown in **Figure 1** and each particle and its vicinity is modeled by a finite element mesh. We call it as "local finite element model" or "local model". To distribute many particles as depicted in **Figure 1**, we simply place the local models in the analysis region by specifying their locations. A unit cell or a structure as whole made of the composite is discretized by a coarse finite element model. We call this model as "global finite element model" or "global model" in this paper. We then allow the local models to overlap each other. Therefore the distribution of the particles can arbitrarily be specified. If the material within the particle is specified to be very soft compared with the matrix material, we can model a porous material.

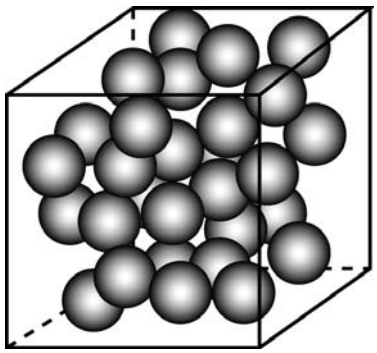

Figure 1 : Particulate composite material with randomly distributed filled particles

In this paper, we present formulations and some numerical results for two- and three-dimensional elastic problems. It is noted that the method is to be extended to deal with elastic-plastic as well as elastic-viscoplastic materials. The extensions will be presented in the authors' forthcoming papers.

2 Mathematical Formulations

It is assumed that particles or voids distribute in the domain of analysis as shown in **Figure 1**. Though **Figure 1** implies that the particles or voids are spherical in their shapes, there is no such restrictions in the mathematical formulation. The second phase material or voids can be fibrous or any others in their shapes. Though the previous formulations of S-FEM (see Fish (1992) for example) assumes only one overlaid model to be superposed

on the global model, we allow any numbers of finite element models to be superposed on the global one. Then, the overlaid models are allowed to overlap each other, as depicted in **Figure 2**. When the shapes of the embedded second phase materials are the same or similar to each other, the same local finite element model can be used repeatedly. Therefore, generating a model for the particulate composite material would be a simple task.

In the following discussions, the regions of the global and the p-th (p=1,2,3, $\cdots$, n) local finite element models are designated to be Ω^G and Ω^{Lp}, as depicted in **Figure 3**. We assume that there are a total of n local model regions. The displacement are defined based on the shape functions of elements in the global and local models, independently [see references such as Bathe (1996) and Hughes (1987) for the shape functions of finite elements]. We write them, as $u_i^G = u_i^G(\mathbf{x})$ in Ω^G and $u_i^{Lp} = u_i^{Lp}(\mathbf{x})$ in Ω^{Lp}, where $\mathbf{x}$ denotes the position of a material point. At a point which is outside all the local model regions, the displacements u_i are the same as the displacement functions u_i^G of Ω^G.

$$u_i = u_i^G(\mathbf{x}) \tag{1}$$

At a point where some local finite element models overlap, the displacement functions u_i are given by the sum of displacement functions of the overlapped models. For example, at a point where the local models Ω^{Lp} and Ω^{Lq} $(1 \le p,q \le n,\ p \ne q)$ overlap on the global model Ω^G, the displacements u_i are represented by the sum of their displacement functions, as:

$$u_i = u_i^G(\mathbf{x}) + u_i^{Lp}(\mathbf{x}) + u_i^{Lq}(\mathbf{x}) \tag{2}$$

To ensure the continuities of displacements, those based on a local finite element model are set to be zero at its outer boundary. We let:

$$u_i^{Lp} = 0 \ \text{ at } \ \partial\Omega^{Lp} \tag{3}$$

where $\partial\Omega^{Lp}$ designates the outer boundary of local finite element region Ω^{Lp}.

Stresses at a point are written in terms of strains through Hooke's law [see Sokolnikoff (1956), for example].

$$\sigma_{ij} = E_{ijk\ell}\varepsilon_{k\ell} \tag{4}$$

The elastic constants may vary within the solid and are the functions of location of a material point.

$$E_{ijk\ell} = E_{ijk\ell}(\mathbf{x}) \tag{5}$$

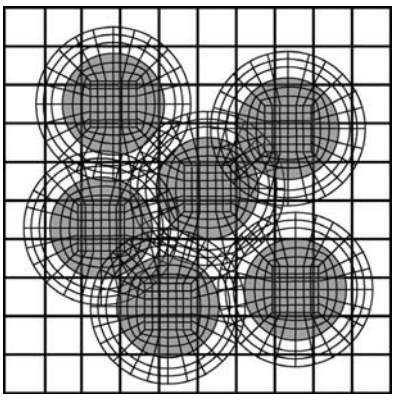

Figure 2 : Two-dimensional illustration for how a composite material is modeled by proposed element overlay technique

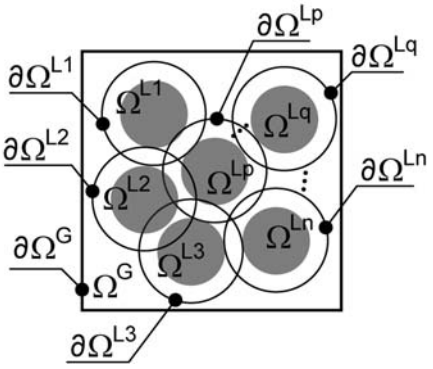

Figure 3 : The domains and boundaries of global model and local models

The statement of principle of virtual work is written to be:

$$\int_{\Omega^G} \frac{\partial \delta u_i}{\partial x_j} E_{ijk\ell} \frac{\partial u_k}{\partial x_\ell} \mathrm{d}\Omega^G = \int_{\Omega^G} \delta u_i b_i \mathrm{d}\Omega^G + \int_{\partial\Omega_t^G} \delta u_i \bar{t}_i d\left(\partial\Omega_t^G\right) \tag{6}$$

where δu_i are the variations of displacements, b_i are the body force per unit volume, $\bar{t}_i$ are the prescribed traction vector on the traction prescribed boundary $\partial\Omega_t^G$. The variations of displacements δu_i are assumed in the same manner as the displacements u_i, by the superposition at material points where they overlap. Thus, δu_i are written to be $\delta u_i = \delta u_i^G(\mathbf{x})$ where no local models overlap on the global model and $\delta u_i = \delta u_i^G(\mathbf{x}) + \delta u_i^{Lp}(\mathbf{x}) + \delta u_i^{Lq}(\mathbf{x})$

where local models Ω^{Lp} and Ω^{Lq} $(1 \le p,q \le n,\ p \ne q)$ overlap on the global model. $\delta u_i^p \quad (1 \le p \le n)$ are set to be zero at the boundary $\partial\Omega^{Lp}$ of Ω^{Lp}.

Thus, the displacements and their variations are substituted in the statement of virtual work principle. After some algebraic manipulations, we arrive at:

$$\int_{\Omega^G} \frac{\partial \delta u_i^G}{\partial x_j} E_{ijk\ell} \frac{\partial u_k^G}{\partial x_\ell} \mathrm{d}\Omega^G + \sum_{p=1}^{n} \int_{\Omega^{Lp}} \frac{\partial \delta u_i^G}{\partial x_j} E_{ijk\ell} \frac{\partial u_k^{Lp}}{\partial x_\ell} \mathrm{d}\Omega^{Lp} = \int_{\Omega^G} \delta u_i^G b_i \mathrm{d}\Omega^G + \int_{\partial\Omega_t^G} \delta u_i \bar{t}_i \mathrm{d}\left(\partial\Omega_t^G\right) \tag{7}$$

$$\int_{\Omega^{Lp}} \frac{\partial \delta u_i^{Lp}}{\partial x_j} E_{ijk\ell} \frac{\partial u_k^G}{\partial x_\ell} \mathrm{d}\Omega^{Lp} + \int_{\Omega^{Lp}} \frac{\partial \delta u_i^{Lp}}{\partial x_j} E_{ijk\ell} \frac{\partial u_k^{Lp}}{\partial x_\ell} \mathrm{d}\Omega^{Lp} + \sum_{\substack{q=1 \\ q\ne p}}^{n} \int_{\Omega^{Lp-Lq}} \frac{\partial \delta u_i^{Lp}}{\partial x_j} E_{ijk\ell} \frac{\partial u_k^{Lq}}{\partial x_\ell} \mathrm{d}\Omega^{Lp-Lq} = \int_{\Omega^{Lp}} \delta u_i^{Lp} b_i \mathrm{d}\Omega^{Lp} \qquad (p = 1,2,3,\cdots,n) \tag{8}$$

From the right hand sides of equations (7) and (8), various stiffness matrices are obtained. Thus, an equation in a matrix form can be written, as:

$$\begin{bmatrix} \mathbf{K}^G & \mathbf{K}^{G-L1} & \mathbf{K}^{G-L2} & \mathbf{K}^{G-L3} & \cdots & \mathbf{K}^{G-Ln} \\ \mathbf{K}^{L1-G} & \mathbf{K}^{L1} & \mathbf{K}^{L1-L2} & \mathbf{K}^{L1-L3} & \cdots & \mathbf{K}^{L1-Ln} \\ \mathbf{K}^{L2-G} & \mathbf{K}^{L2-L1} & \mathbf{K}^{L2} & \mathbf{K}^{L2-L3} & \cdots & \mathbf{K}^{L2-Ln} \\ \mathbf{K}^{L3-G} & \mathbf{K}^{L3-L1} & \mathbf{K}^{L3-L2} & \mathbf{K}^{L3} & \cdots & \mathbf{K}^{L3-Ln} \\ \vdots & \vdots & \vdots & \vdots & \ddots & \vdots \\ \mathbf{K}^{Ln-G} & \mathbf{K}^{Ln-L1} & \mathbf{K}^{Ln-L2} & \mathbf{K}^{Ln-L3} & \cdots & \mathbf{K}^{Ln} \end{bmatrix} \begin{Bmatrix} \mathbf{u}^G \\ \mathbf{u}^{L1} \\ \mathbf{u}^{L2} \\ \mathbf{u}^{L3} \\ \vdots \\ \mathbf{u}^{Ln} \end{Bmatrix} = \begin{Bmatrix} \mathbf{b}^G \\ \mathbf{b}^{L1} \\ \mathbf{b}^{L2} \\ \mathbf{b}^{L3} \\ \vdots \\ \mathbf{b}^{Ln} \end{Bmatrix} + \begin{Bmatrix} \mathbf{f}^G \\ \mathbf{0} \\ \mathbf{0} \\ \mathbf{0} \\ \vdots \\ \mathbf{0} \end{Bmatrix} \tag{9}$$

$\mathbf{K}^G$ is the ordinary stiffness matrix for the global finite element model which arises from the first of equation (7) and $\mathbf{K}^{Lp} \quad (p = 1,2,3,\cdots,n)$ are those for the local finite element models arising from the second of equation (8). $\mathbf{K}^{G-Lp} \quad (p = 1,2,3,\cdots,n)$ and $\mathbf{K}^{Lp-G} \quad (p = 1,2,3,\cdots,n)$ are the coupling stiffness matrices between the global and local finite element models, arising from the second of equation (7) and the first of equation (8), respectively. $\mathbf{K}^{Lp-Lq} \quad (p,q = 1,2,3,\cdots,n;\ p \ne q)$ are the coupling stiffness matrices between the local finite element models arising from the third of equation (8). $\mathbf{b}^G$ and $\mathbf{b}^{Lp} \quad (p = 1,2,3,\cdots,n)$ are the resulting nodal forces of the body force terms. $\mathbf{f}^G$ is the nodal force vector of external forces. It is noted that the matrices have the symmetric properties of $\mathbf{K}^{Lp-G} = \left(\mathbf{K}^{G-Lp}\right)^T$ and $\mathbf{K}^{Lp-Lq} = \left(\mathbf{K}^{Lq-Lp}\right)^T$. Therefore, the coefficient matrix of the left hand side of equation (9) is symmetric.

3 Computational Procedures for Heterogeneous Materials

3.1 Material Constants

As done in an ordinary finite element analysis, material constants such as Young's modulus are specified based on finite elements. In present case, the local finite element models represent the material heterogeneities. Thus, the material properties are specified such that, the global finite element model has the material properties of matrix material only and the materials other than matrix material are specified in the local finite element model. Therefore, there are regions where two or more different materials are specified by the global and local finite element models. A typical scenario is presented in **Figure 4** for a two-dimensional illustrative example. There are two local finite element models. Each local finite element model has a region corresponding to a particle where the material constants are different from those of matrix material. In the figure, they are designated as "matrix material", "particle type 1" and "particle type 2". We assign priority orders to the materials. Their priorities are in the order of "particle type 2", "particle type 1" and "matrix material". Thus, at a point where all of three overlap "particle type 2" is chosen as it has the highest priority order among the three. At a point where "particle type 2" and "matrix material" overlap, "particle type 2" is used as it has higher priority order than the other. The priority orders are given to material models as input data.

3.2 Integration for Coupling Stiffness Matrices

In present approach, finite elements overlap each other. There are three kinds of ways that elements overlap each

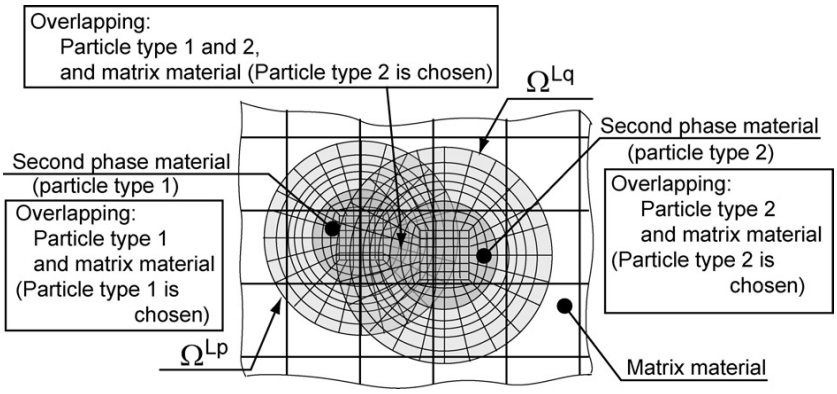

Figure 4 : A schematic illustration for how material models are specified and how an appropriate one is chosen in the element overlay technique

other. There are three cases; i) an element is completely inside the other, ii) two elements partially overlap and iii) an element completely include the other, as shown in **Figure 5**. In **Figure 5**, the *s*-th element of the *p*-th local finite element model overlaps with the *t*-th element of the *q*-th local finite element. They are designated as "$EL(p,s)$" and "$EL(q,t)$", respectively. The volumes (areas) of the two elements are denoted to be $\Omega^{(p,s)}$ and $\Omega^{(q,t)}$. Coupling stiffness matrix $\left[\mathbf{k}^{(p,s)-(q,t)}\right]$ between the two elements can be written to be:

$$\left[\mathbf{k}^{(p,s)-(q,t)}\right] = \int_{\Omega^{(p,s)-(q-t)}} \left[\mathbf{B}^{(p,s)}\right]^T [\mathbf{E}] \left[\mathbf{B}^{(q,t)}\right] \mathrm{d}\Omega^{(p,s)-(q,t)} \qquad (10)$$

where $\Omega^{(p,s)-(q,t)}$ is the volume (area) that is shared by the two elements. $\left[\mathbf{B}^{(p,s)}\right]$ and $\left[\mathbf{B}^{(q,t)}\right]$ are the strain-displacement matrices of $EL(p,s)$ and $EL(q,t)$, respectively.

When $EL(p,s)$ is completely inside of $EL(q,t)$ [case (i)], the integration is carried out based on $\Omega^{(p,s)}$ and when $EL(q,t)$ is inside of $EL(p,s)$ [case (iii)], quadrature rule is applied to $\Omega^{(q,t)}$. However, for the case (ii) that $\Omega^{(p,s)}$ and $\Omega^{(q,t)}$ partially overlap each other, an ordinary quadrature rule can not be applied to $\Omega^{(p,s)-(q,t)}$, as its shape may be very complex. In **Figure 5 (b)**, a two dimensional case is illustrated and the geometry of overlapping region looks to be simple. However, the shape of overlapping region in three-dimensional cases would be much more complex than the two-dimensional case, as shown in **Figure 6**. There are many ways for these elements to overlap. In this paper, a simple algorithm that works for both two- and three-dimensional problems is developed to perform the integration accurately.

We rewrite equation (10), as:

$$\begin{aligned}\left[\mathbf{k}^{(p,s)-(q,t)}\right] &= \int_{\Omega^{(p,s)}} \Theta^{(p,s)-(q,t)}(\mathbf{x}) \left[\mathbf{B}^{(p,s)}\right]^T [\mathbf{E}] \left[\mathbf{B}^{(q,t)}\right] \mathrm{d}\Omega^{(p,s)} \quad \text{or} \\ &= \int_{\Omega^{(q,t)}} \Theta^{(p,s)-(q,t)}(\mathbf{x}) \left[\mathbf{B}^{(p,s)}\right]^T [\mathbf{E}] \left[\mathbf{B}^{(q,t)}\right] \mathrm{d}\Omega^{(q,t)} \qquad (11)\end{aligned}$$

Here, integration is performed for the region of *EL(p,s)* or of *EL(q,t)*. $\Theta^{(p,s)-(q,t)}(\mathbf{x})$ is a function of $\mathbf{x}$, whose value is one inside the region of $\Omega^{(p,s)-(q,t)}$. Otherwise, it takes zero. Therefore, the integrands in equation (11) would have sever discontinuities. An ordinary Gauss quadrature that is usually adopted in finite element programs would fail to serve accurate results. Fish (1992) proposed the use of ordinary Gauss quadrature rule to carry out the integration of equation (11). It must be pointed out here that in present applications, ways that elements overlap each other are much more complex than what was assumed in Fish (1992), as the local finite element models are allowed to overlap. Therefore, the accuracy of the integration has a more pronounced influence on the solutions. Readers are referred to Okada, Endoh and Kikuchi (2004) in which the influence of quadrature rule on the accuracy of S-FEM analysis was discussed.

In **Figure 7**, a two-dimensional example is presented. $EL(p,s)$ partially overlaps with $EL(q,t)$ and the integral is performed based on $EL(p,s)$. First, $EL(p,s)$ is divided into four subdivisions. Each subdivision is checked if any of edge line intersects with it. If an intersection is de-

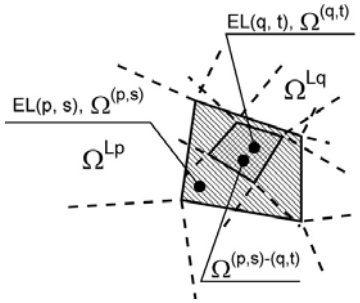

(a) case (i): *EL(q,t)* is completely included in *EL(p,s)*

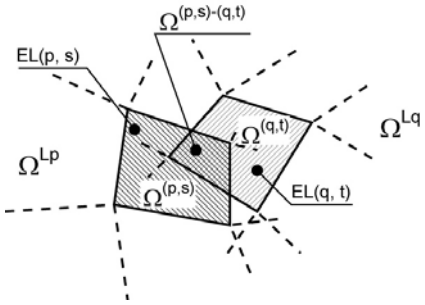

(b) case (ii): *EL(q,t)* and *EL(p,s)* partially overlap

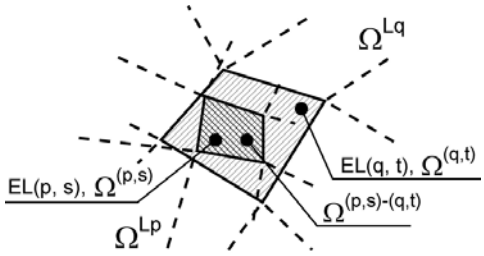

(c) case (iii) *EL(p,s)* is completely included in *EL(q,t)*

Figure 5 : The *s*-th element of the *p*-th local model overlaps with the *t*-th element of the *q*-th local model

tected, the subdivision is divided again. Then, each subdivision of $EL(p,s)$ is checked at its center if it is inside of $EL(q,t)$. Then, the volume of $\Omega^{(p,s)-(q,t)}$ is computed. This process is repeated until the change of computed volume of $\Omega^{(p,s)-(q,t)}$ becomes small enough compared with the volume (area) of $EL(p,s)$. In present analyses, the subdivisions are carried out until the change of computed volume of $\Omega^{(p,s)-(q,t)}$ becomes less than 1% and 0.1% for two- and three-dimensional problems, respectively.

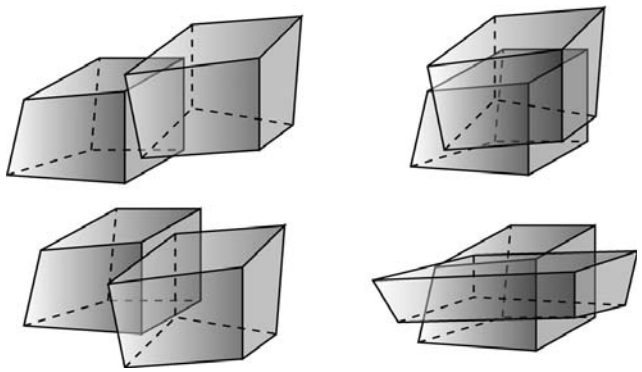

Figure 6 : Many ways that two three-dimensional hexahedron elements overlap each other

3.3 Solution Procedure for the Linear Simultaneous Equation (9)

Equation (9) is solved for unknown displacements. The coefficient matrix of the right hand side of equation (9) does not have a band structure. Therefore, linear equation solvers for band matrix that are popular for finite element calculations would not be very efficient in terms of computer memory usage. Thus, we adopted an iterative solver (Pre-conditioned conjugate gradient method) that requires only non-zero elements of coefficient matrix to be stored in computer memory [see, for example, Oguni, Murata, Miyoshi, Dongarra and Hasegawa (1991)].

4 Accuracy of S-FEM Analysis

In this chapter, we discuss about the accuracy of present S-FEM analysis by taking some simple cases as our example problems. Circular hole and spherical void problems are solved and their solutions are compared with their analytical ones. As a governing factor for the accuracy of analysis, the connection of displacement field from the global to local finite element model may have a large impact on the accuracy of results. Thus, the sizes of stress concentration source (i.e., hole), local mesh region and elements in global model need to be set appropriately. We try to come up with simple guidelines to perform present S-FEM analysis accurately.

Material in the hole/void is modeled as an elastic material whose Young's modulus is much smaller than that of the surrounding. In this way, the same local finite ele-

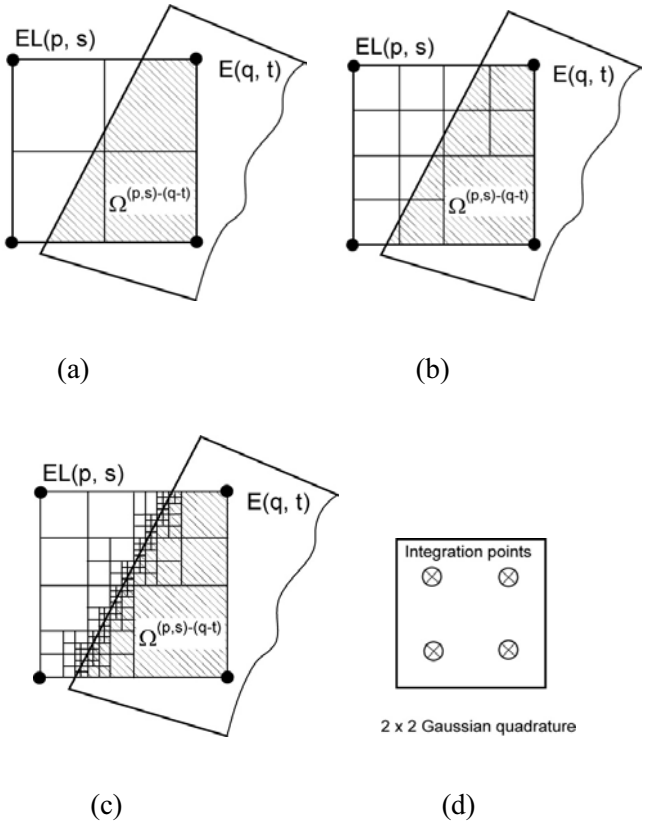

Figure 7 : Element subdivision technique for integrating stiffness matrices [(a) First step: element EL(p, s) is divided into four subdivisions, (b) Subdivisions that the boundary of element EL(q,t) runs through are divided further, (c) Further subdivisions, (d) Integration points for each subdivision]

ment model can be used for the problems of stiffer particles just by changing the value for Young's modulus. Material constants that are used in present analyses are summarized in **Table 1**.

Table 1 : Young's moduli and Poisson's ratio assumed for the circular hole/spherical void problems

	Young's modulus	Poisson's ratio
Surrounding Material (Matrix)	E	0.3
In Circular Hole/Spherical Void	E / 100	0.3

4.1 One Circular Hole Problem (Two-Dimensional Problem)

Stress concentration associated with a circular hole in a large panel is analyzed by proposed S-FEM approach. As shown in **Figure 8**, a hole is placed in a very large panel. Then, the panel is subject to tension. Stress distributions along the edge of the circular hole are compared between those computed by present S-FEM analyses and analytical solution [see, for example, Sokolnikoff (1956)].

Typical global and local finite element models are presented in **Figure 9**. The shape of local model region is circular and its radius is denoted by *R*. The radius of hole is denoted by *r*. The global finite element model is consisting of square shaped finite elements. The length of each edge of a global element is denoted by *Lg*. Both for global and local finite element models, four node linear elements are adopted.

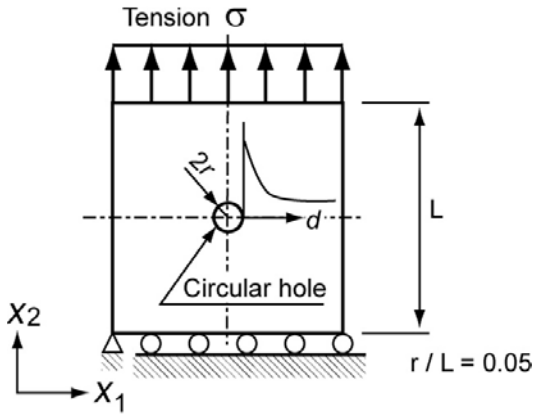

Figure 8 : Circular hole problem to evaluate the accuracy of proposed methodology

A number of analyses are carried out by using present S-FEM program with changing the ratios *R*/*Lg* and *R*/*r*. The radius *r* and size *L* of hole and of square block are set to be 0.5 mm and 10 mm, respectively. Results for the ratio *r*/*Lg* being 3.34, 2 and 1.25 are presented in **Figure 10 (a)**, **(b)** and **(c)**, respectively. It is seen from **Figure 10 (a)** that when the ratio *R*/*Lg* is less than one, the stress concentration at the edge of crack is not appropriately reproduced. In these cases, the ratio *R*/*r* varies from 1.5 to 3.0. In **Figure 10 (b)**, except for the case *R*/*Lg* is set to be 0.75, the solutions are similar. The ratios *R*/*r* in these cases are from 1.5 to 3.0. **Figure 10 (c)** indicates that for

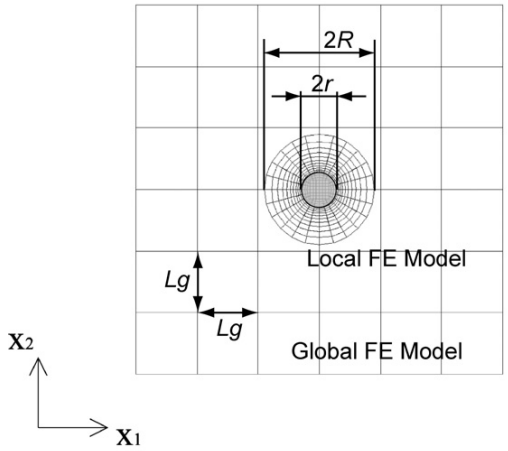

Figure 9 : A typical global and local finite element model for the circular hole problem

all the cases *R*/*Lg* equals 1.2 or greater, the solutions are close to the analytical curve. In these cases, *R*/*r* varies from 1.5 to 3.0. These results indicate that when the ratio *R*/*Lg* equals or greater than 1.0, the solutions are accurate, almost regardless of the ratio *R*/*r*. Thus, we investigated how the ratio *R*/*r* influences the accuracy of solution and the results are shown in **Figure 11**. In **Figure 11**, the ratio *R*/*Lg* equals 1.0 and *R*/*r* varies from 1.25 to 3.34. It is seen that, except for the case of *R*/*r* being 1.25, data points fall on a curve, which is slightly off from the analytical curve. The case that *R*/*Lg* and *R*/*r* equal 1.2 and 1.5, respectively, give accurate solutions, as seen in **Figure 10 (c)**. It can be concluded from these results that the ratios *R*/*Lg* and *R*/*r* should be equal or greater than 1.0 and 1.5, respectively. That is the guideline to carry out present S-FEM analysis accurately, provided that the discretization for local model is fine enough.

4.2 Four Circular Hole Problem (Two-Dimensional Problem)

In this section, the accuracy of solution when the local models overlap each other is considered. The solution of present S-FEM analysis is compared with that of an ordinary finite element program. In **Figure 12**, the arrangements of circular holes and local finite element models are depicted. The local finite element models overlap each other. Global and local finite element models that are used in this analysis are given in **Figure 13**. In both S-FEM and ordinary FEM analyses, material in the circular holes is modeled as an elastic material whose Young's modulus is much smaller than that of the surrounding, as summarized in **Table 1**. Four node linear elements

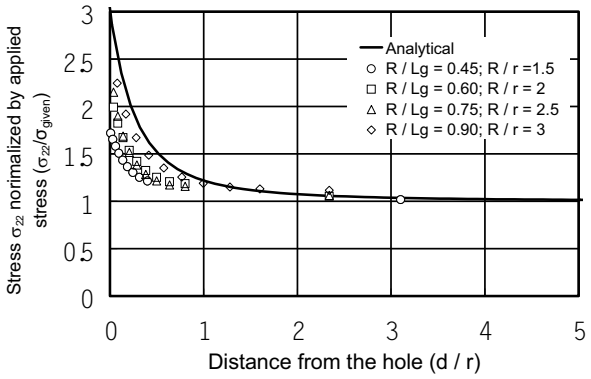

(a) $Lg / r = 3.34$

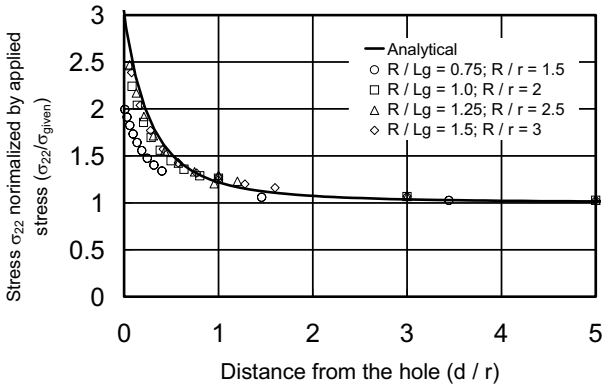

(b) $Lg / r = 2$

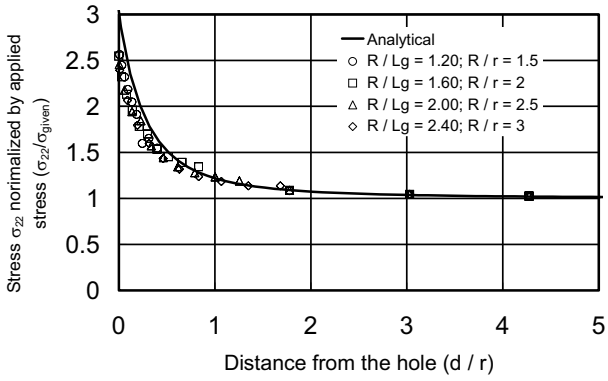

(c) $Lg / r = 1.25$

Figure 10 : The variations of stress σ_{22} normalized by applied stress σ computed by various size ratios between *Lg*, *R* and *r*

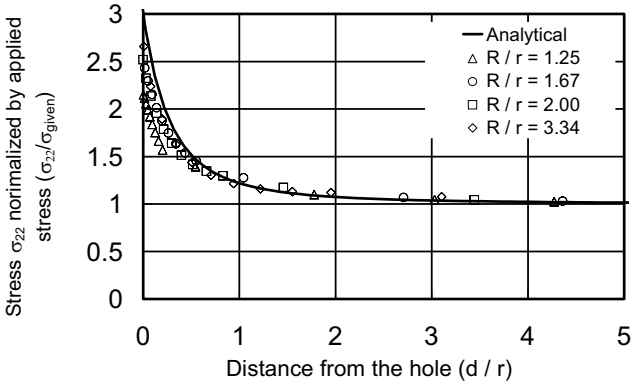

Figure 11 : The variations of stress σ_{22} normalized by applied stress σ, for Lg / R = 1 with various ratios of R / r

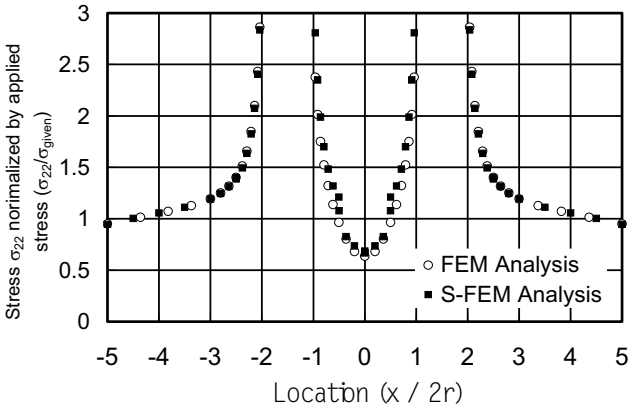

Figure 14 : Distribution of stress σ_{22} normalized by the applied stress, along the line A-A'

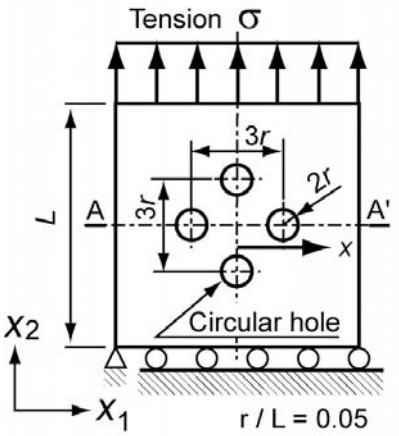

Figure 12 : Four circular hole problem.

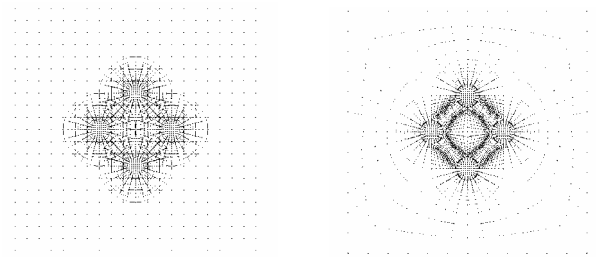

(a) S-FEM model (b) Ordinary FEM model

Figure 13 : S-FEM and ordinary finite element models for the four circular hole problem

are adopted for the analyses. The model for ordinary finite element analysis has a total of 2576 and 2601 elements and nodes. The global finite element model for S-FEM analysis has 144 elements and 169 nodes. The local model has 980 elements and 1001 nodes.

In **Figure 14**, the distribution of stress in the tensile direction along the line A-A' in **Figure 12**, is presented. The solution of an ordinary finite element program is plotted as a reference solution. The solutions of present S-FEM and the ordinary finite element method are very close to each other.

4.3 Spherical Void Problem (Three-Dimensional Problem)

A spherical void is placed at the center of analysis region. The analysis region is large compared with the size of spherical void. R, r and Lg represent the radii of local mesh region and spherical void and the edge length of each global element, respectively. As depicted in **Figure 15**, the radius r of spherical void and the size L of cubical analysis region are set to be 0.5 mm and 10 mm, respectively. A typical analysis model including global and local finite element models is shown in **Figure 16** for its cross section. Global finite element model is consisting of cubical shaped finite elements. Local finite element model region has a spherical shape and its radius R is varied. We then performed a number of analyses for various combinations of ratios R/r and R/Lg. Material in the void is modeled as an elastic material whose Young's modulus is much smaller than that of the surrounding, as summarized in **Table 1**. Both for global and local finite element models, eight node linear elements are adopted.

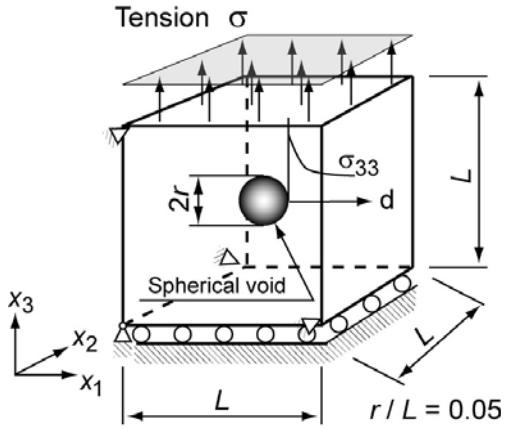

Figure 15 : A cube containing a spherical void at its center subject to tension

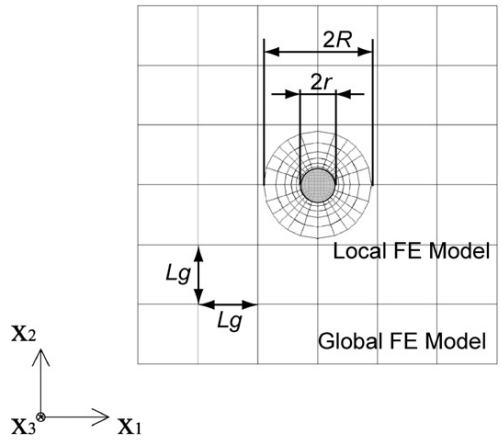

Figure 16 : The cross section of a typical S-FEM analysis model for the problem of one spherical void in a cubical block

In **Figure 17 (a)**, **(b)** and **(c)**, the variations of computed stress in the tensile direction along a horizontal line from the edge of the void are compared with the analytical solution [see, for example, Nishida (1973)], for the ratio *r*/*Lg* being 3.34, 2 and 1.25, respectively. In **Figure 17 (a)**, results are presented for the ratios *R*/*Lg* and *R*/*r* being 0.45∼0.9 and 1.5∼3.0, respectively. In all the cases presented in **Figure 17 (a)**, the values of stress are not close to the analytical curve. In **Figure 17 (b)**, the ratios *R*/*Lg* and *R*/*r* are varied from 0.75 to 1.5 and from 1.5 to 3.0, respectively. The results when the ratio *R*/*Lg* is less than 1.5, the results somewhat deviate from the curve of

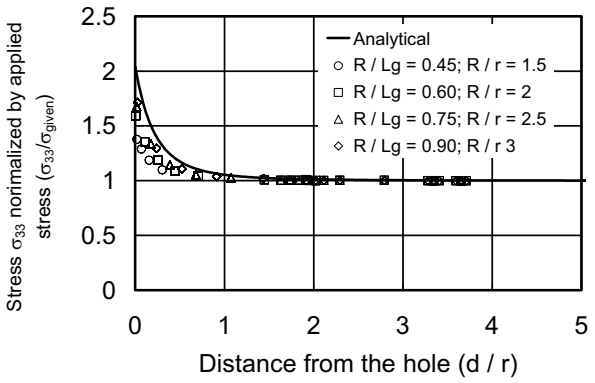

(a) $Lg / r = 3.34$

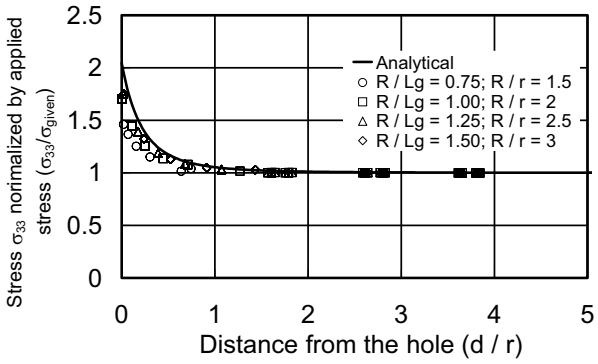

(b) $Lg / r = 2$

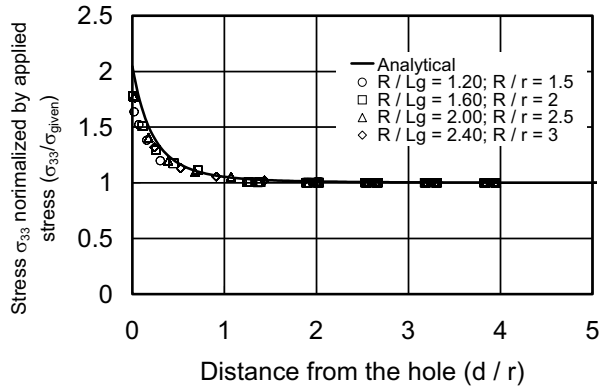

(c) $Lg / r = 1.25$

Figure 17 : The variations of stress σ_{33} normalized by applied stress σ computed by various ratios between *Lg*, *R* and *r*, for the problems of spherical void in a cube

analytical solution. The solutions for the ratio *R*/*Lg* being 1.2∼2.4 are plotted in **Figure 17 (c)**. The solutions are close to the analytical curve. But for *R*/*Lg* being 1.2, the computed stresses are slightly smaller than the other.

By combining the above findings, to obtain accurate solutions, the ratio R/Lg needs to be roughly equal 1.5 or greater. The influence of the ratio R/r to the accuracy of the solution is investigated in **Figure 18**. The ratio R/Lg is fixed to be 1.5. It is found that for all the cases that R/r being 1.25∼3.0, the stress concentration at the sides of the hole is reproduced. However, for R/r=1.25, a large discrepancy from the analytical curve is seen at d/r =1.5. This is because, this point is outside the local finite element model and the stress is only based on the global model. There are some points like this for R/r=1.5 also.

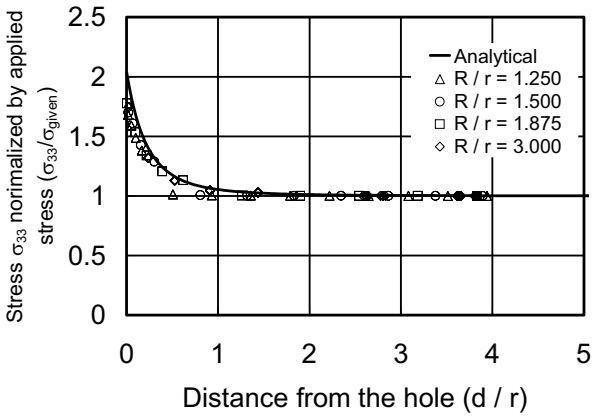

Figure 18 : The variations of stress σ_{33} normalized by applied stress σ, for Lg / R = 1.5 with various ratios of R / r

Combining discussions above, R/Lg and R/r should be equal or greater than 1.5 and 1.5, respectively, to carry out the three-dimensional S-FEM analysis accurately.

4.4 Discussions on the Accuracy of S-FEM for Stress Concentration Problems

From the results that are presented in this chapter, we can draw some conclusions as guidelines to perform present S-FEM analyses for stress concentration problems accurately.

The solutions are very sensitive to how large the local finite element model region is. For two- and three-dimensional cases, the sizes (radii) of the local model regions should be the same and 1.5 times larger than the size of a global element, respectively. The size of local mesh region relative to that of hole/void also influences the accuracy of solution. Furthermore, it has been demonstrated that superposing two or more local mesh regions together does not deteriorate the accuracy of the solutions, as seen in the four hole problem.

5 The Problems of Distributed Holes/Voids and Stiff Particles

In this chapter, some example problems are presented and the capabilities of present S-FEM technique are demonstrated. Holes/voids and particles are distributed randomly by using Sobol' sequence [Press, Teukolsky, Vetterling and Flannery (1996)], which is a method to evenly distribute points in a multi dimensional space. In present analyses, we generate models for the specified radii of holes/voids. When points are generated by using Sobol' sequence, the particles may overlap each other and some local finite element models may intersect with the outer boundary of the global model region. In present study, we simply omit such locations from placing the holes/voids and particles, except for a few places in two-dimensional example problem. Therefore, holes/voids and particles do not overlap each other and all the local finite element models are contained in the region of global finite element model. Both for global and local finite element models, four and eight node linear elements are adopted for two- and three-dimensional analyses, respectively.

5.1 250 Hole/Particle Problems in Two-Dimensional Tension Block

First, the results of two-dimensional problems are presented. 250 holes/stiff particles are distributed in a 10 x 10 (mm) square region, as depicted in **Figure 19**. The radii of each holes/particles are 0.15 mm and their fraction is 17.6%. A few holes/particles overlap each other. Holes are modeled as extremely soft elastic material. The Young's moduli of hole and particle regions are set to be 1/100 and 10 times of that of matrix material. The square shaped plate is subject to a uniform tension at its top, as shown in **Figure 19**. In **Figure 19**, the global and local finite element models are also presented. There are a total of 372 and 385 elements and nodes for each local finite element model and the global model has a total of 400 and 441 elements and nodes.

In **Figure 20**, the distributions of stress are presented for the hole and particle problems. The distributions are shown in gray-scale in which dark and light colors indicate the location of high and low stress, respectively.

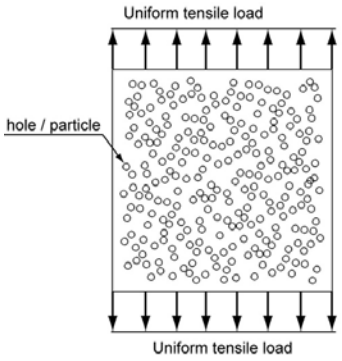

(a) Arrangement of holes/particles.

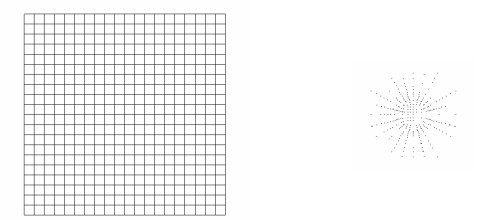

(b) Global finite element model (c) Local finite element model

Figure 19 : The arrangement of holes/particles and the global and local finite element models for 250 hole/particle problem

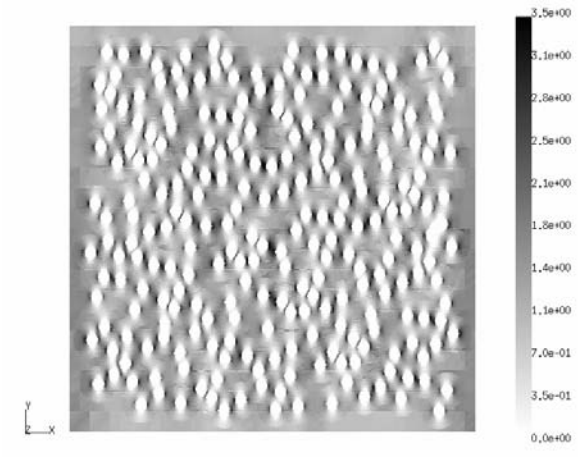

(a) 250 holes

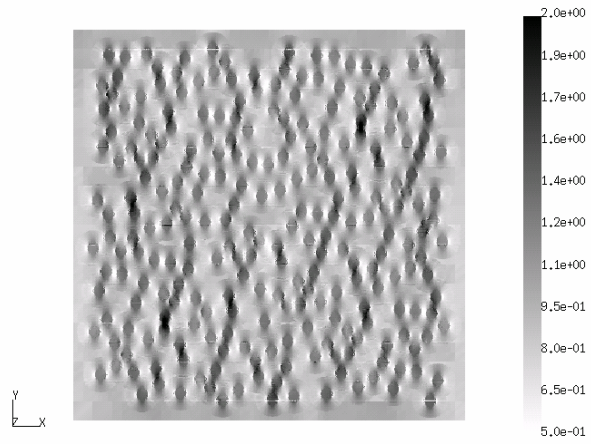

(b) 250 particles

Figure 20 : The distribution of stress σ_{22} normalized by applied tensile stress σ for 250 hole/particle problem

In **Figure 20 (a)**, the result for the hole problem is presented and it is seen that stress concentrates at the sides of holes. The magnitudes of stress concentration seem to vary due to the distribution of holes. At the top and bottom of each hole, stress is almost zero and stress is very low between the holes when they align in vertical direction. In **Figure 20 (b)**, the result of the particle problem is presented. Stress inside the holes is high and the high stress regions extend in vertical direction in matrix material. When the particles align in vertical direction, the high stress regions connect the particles. The magnitude of stress rise seem to be influenced by the distribution of particles.

5.2 35 Void/Particle Problems in Three-Dimensional Tension Block

In **Figure 21**, a three-dimensional model containing 35 voids/particles in a 10 x 10 x 10 (mm) cubical block is shown. The radii of voids/particles are 0.8 mm and their volume fraction is 7.5%. The Young's moduli of voids and particles are set to be 1/100 and 10 times of that of matrix material. The global and local finite element models are also shown in **Figure 21**. There are a total of 928 and 1007 elements and nodes for each local finite element model. The global model has 1000 elements and 1331 nodes. In **Figure 22**, stress distributions for the void and particle problems in a section through the block are shown.

The stress concentrations are seen at both the sides of voids and at top and bottom of particles. In addition, there are many particles/particles just behind and above the plane of visualization. Thus, the stress distributions in the section are very complicated. Stress concentrations and decreases due to the unseen voids/particles appear in

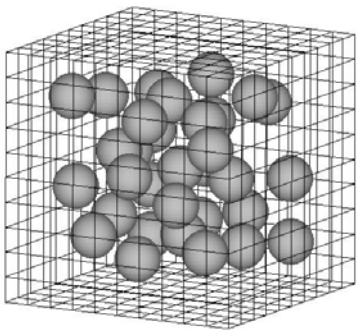

(a) 35 void/particle model (arrangement of voids/particles and 10x10x10 global finite element model)

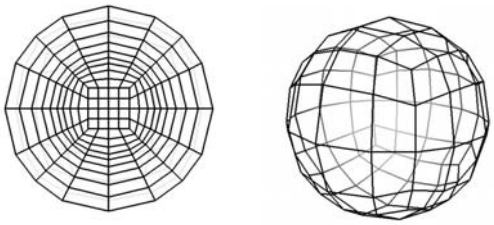

(b) Local finite element model (cut model and outside)

Figure 21 : The arrangement of holes/particles and the global and local finite element models for 35 void/particle problem

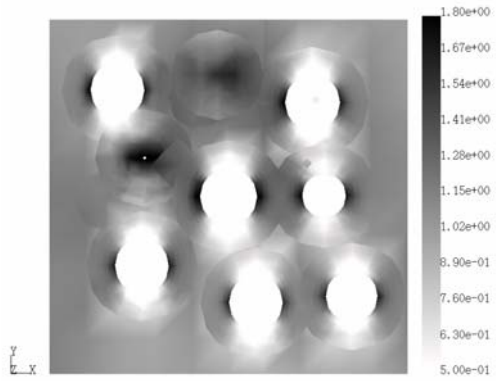

(a) 35 hole problem

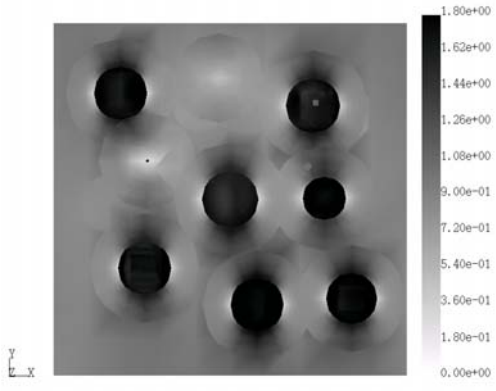

(b) 35 particle problem

Figure 22 : The distributions of stress σ_{22} normalized by applied tensile stress σ for 35 hole/particle problem

the stress distributions.

6 Discussions and Concluding Remarks

In this paper, an element overlay technique (S-FEM) for problems containing many distributed voids and filled particles is developed. Many local finite element models are superposed on the global model and they are allowed to overlap each other. Each local finite element model represents a void or a particle. When the voids/particles have the same geometry, the same local finite element model can be used repeatedly. Therefore, building/changing a model containing many voids/particles is a trivial task. Present approach can be used to investigate the detailed deformation behavior of porous/composite materials with complex internal structures.

A simple criterion to perform present S-FEM analysis accurately is proposed. That is, the size of local finite element region should be large enough compared with that of an element in the global finite element model. For two-dimensional cases, the representative size of local mesh region needs to be the same as or larger than that of global element. For three-dimensional problems, the size of local mesh region must be slightly larger than the two-dimensional cases. The size must be about 1.5 times larger than the size of an element in the global model. A similar finding was presented by Okada, Endoh and Kikuchi (2004) for two-dimensional fracture mechanics problems. Furthermore, it was demonstrated in this paper that even when several local finite element models are overlapped each other, the results are accurate.

Combining the outcomes of present research, we can perform mesoscopic analyses on particulate composite materials accurately with much less modeling efforts compared with the case of ordinary finite element method. We have demonstrated 250 hole/particle and

35 void/particles problems in two- and three-dimensional unit cell. We will then extend present work to perform nonlinear/damage analyses in which the influence of randomness in void/particle arrangement would be more pronounced than linear elastic problems. We are now developing an S-FEM computer program that enables material nonlinear (elastic-plastic and elasto-viscoplastic) analysis. However, as discussed in this paper, the computation for coupling stiffness matrix still has some numerical difficulties. Although the method that is described in this paper works in terms of numerical accuracy, the developed numerical technique takes considerable amount of computational time as the number of integration points is so large. This issue needs to be attacked and will be reported by the authors in near future.

Acknowledgement: The work presented in this paper has been supported by AOARD (Asian Office of Aerospace Research and Development) (AOARD02-4012, 03-4012, 04-4012). The authors would like to express their sincere gratitude to the support and to the encouragement of Dr. K. Goretta of AOARD.

References

Atluri, S. N. (2004): The meshless method (MLPG) for domain & BIE discretizations, Tech Science Press, Forsyth, GA.

Atluri, S. N.; Shen, S. (2002): The meshless local Petrov-Galerkin (MLPG) method: a simple & less-costly alternative to the finite element and boundary element Methods. *CMES: Computer Modeling in Engineering & Sciences*, vol. 3, no. 1, pp. 11-51.

Bathe, K.-J. (1996): Finite element procedures, Prentice-Hall, Inc., Upper Saddle River, NY.

Böhm, H. J.; Han, W.; Eckschlager, A. (2004): Multi-inclusion unit cell studies of reinforcement stresses and particle failure in discontinuously reinforced ductile matrix composite. *CMES: Computer modeling in Engineering & Sciences*, vol. 5 no. 1, pp. 5-20.

Böhm, H. J.; Han, W.; Eckschlager, A.; Han, W. (2002): Molti-inclusion unit cell models for metal matrix composites with randomly oriented discontinuous reinforcements. Computational Material Science, vol. 25, pp. 42-53.

Chung S. W.; Choi, Y. J.; Kim, S. J. (2003): Computational simulation of localized damage by finite element remeshing based on bubble packing method. *CMES: Computer Modeling in Engineering & Sciences*, vol. 4, no. 6, pp. 707-718.

Fish, J. (1992): The s-version of the finite element method. *Computers & Structures*, vol. 43 no. 3, pp. 539-547.

Fish, J.; Guttal, R. (1996): The s-version of finite element method for laminated composites. *International Journal for Numerical Methods in Engineering*, vol. 39, pp. 3641-3662.

Fish, J.; Markolefas, S.; Guttal, R.; Nayak, P. (1994): On adaptive multilevel superposition of finite element meshes for linear elastostatics. *Applied Numerical Mathematics*, vol. 14, pp. 135-164.

Hughes, T. J. R. (1987): The finite element method –Linear static and dynamic finite element analysis, Prentice-Hall, Englewood Cliffs, N.J.

Kim, H.-G.; Atluri, S. N. (2000): Arbitrary placement of secondary nodes, and error control, in the meshless local Petrov-Galerkin (MLPG) method. *CMES: Computer Modeling in Engineering & Sciences*, vol. 1, no. 3, pp. 11-32.

Lee, K.; Moorthy, S.; Ghosh, S. (1999): Multiple scale computational model for damage in composite materials. *Computer Methods in Applied Mechanics and Engineering*, vol. 172, pp. 175-201.

Lee, S.-H.; Song, J.-H.; Yoon, Y.-C.; Zi, G.; Belytschko, T. (2004): Combined extended and superimposed finite element method for cracks. *International Journal for Numerical Methods in Engineering*, vol. 59, pp. 1119-1136.

Matsuda, T.; Ohno, N.; Tanaka. H.; Shimizu, T. (2003): Effects of fiber distribution on elastic-viscoplastic behavior of long fiber-reinforced laminates. *International Journal of Mechanical Sciences*, vol. 45, pp. 1583-1589.

Moës, N.; Dolbow, J.; Belytschko, T. (1999): A finite element method for crack growth without remeshing. *International Journal for Numerical Methods in Engineering*, vol. 46, pp. 131-150.

Mura, T. (1982): Micromechanics of defects in solid, Martinus Nijhoff Publications, London.

Nakasumi, S.; Suzuki, K.; Fujii, D.; Ohtsubo, H. (2003): Mixed analysis of shell and solid elements using the overlaying mesh method. *Journal of Marine Science*

and Technology, vol. 7, pp. 180-188.

Needleman, A. (1989): Computational micromechanics. *Theoretical and Applied Mechanics (Germain, Piau, Calillerie, eds.)*, IUTAM, Elsevier Science Publications B.V., North-Holland, pp. 217-240.

Nishida, M. (1973): Stress concentration (Ouryoku Shuchu), Morikita Shuppan Co. Ltd., Tokyo, Japan.

Oguni, T.; Murata, K.; Miyoshi, T.; Dongarra, J. J.; Hasegawa, H. (1991): Software for matrix computations (Gyouretsu Keisan Software), Matuzen, Tokyo, Japan.

Okada, H.; Endoh, S. Kikuchi, N. (2004): On fracture analysis using an element overlay technique. *Engineering Fracture Mechanics*, In press.

Okada, H.; Fukui, Y.; Kumazawa, N. (2003a): A micromechanical analysis of rubber modified epoxy resin. *Key Engineering Materials*, vols. 234-244, pp. 511-516.

Okada, H.; Fukui, Y.; Kumazawa, N. (2003b): Analysis for particulate composite materials undergoing damage and stress induced phase transformation using the boundary element method. *Transactions of the Japan Society of Mechanical Engineering*, series A, vol. 69, no. 687, pp. 61-68.

Okada, H.; Fukui, Y.; Kumazawa, N. (2004): Homogenization analysis for particulate composite materials using the boundary element method. *CMES: Computer Modeling in Engineering & Science*s, vol. 5 no. 2, pp. 135-149.

Press, W. H.; Teukolsky, S. A.; Vetterling, W. T.; Flannery, B. P. (1996): *Numerical Recipes in Fortran 77*, Cambridge University Press, Cambridge, UK.

Raghavan, R.; Ghosh, S. (2004): Adaptive multi-scale computational modeling of composite materials. *CMES: Computer Modeling in Engineering & Science*s, vol. 5 no. 2, pp. 151-170.

Sokolnikoff, I. S. (1956): Mathematical theory of elasticity second edition, McGraw-Hill, New York.

Takano, N.; Zako, M.; Ishizono, M. (2000): Global/local modeling of structures with local heterogeneity. *Transactions of the Japan Society of Mechanical Engineering*, series A, vol. 66, no. 642, pp. 14-21.

Zhong, X. A.; Knauss, W. G. (2000): Effects of particle interaction and size variation onn damage evolution in filled elastmers. *Mechanics of Composite Materials and Structures*, vol. 7, pp. 35-53.